2026 IEEE International Conference on Robotics and Automation (ICRA 2026)
June 1-5, 2026. Vienna, Austria

Design and Validation of a Soft Self-Centering Gripper for Delicate Object Handling

Xiaoqian Zhang, Mario Baggetta, Cristina Piazza, and Giovanni Berselli

***Abstract*— Harvesting, gripping, and handling of fruit and vegetables require end-effectors that ensure grip stability while, at the same time, minimizing surface damage and bruising. Conventional rigid or partially compliant solutions often generate localized load concentrations and require high positioning accuracy, limiting their effectiveness in unstructured environments. This work presents a novel three-finger gripper with a self-centering closing mechanism and soft fingers. The system operates in two stages: first, the fingers slide (FS) along linear guides driven by a dedicated motor to adapt to the object size; second, a separate motor actuates the finger closure to establish the grasp. The finger design is inspired by the handed-shearing auxetic (HSA) actuator, enabling controlled pre-shaping (PS) by adapting to the object geometry. The proposed design was first validated through finite element simulations, comparing pre-shaping (PS) against passive compliance (PC) under matched load conditions. Results demonstrate that PS significantly improves pressure uniformity and grasp stability. A fully functional prototype was then fabricated via additive manufacturing.**

***Index Terms*— Soft robotic grippers, self-centering grippers, pre-shaping, compliant mechanisms.**

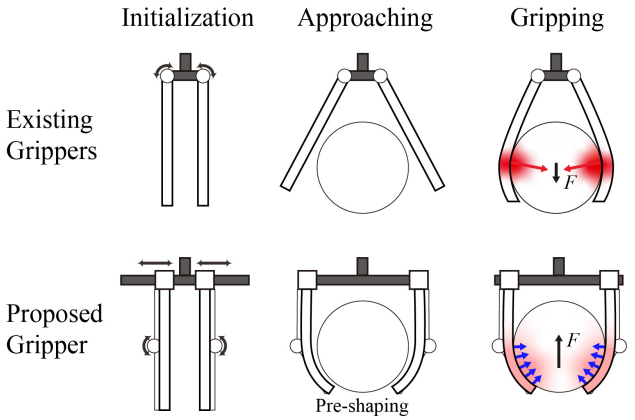

Fig. 1. Conceptual comparison of gripper operation. Existing soft grippers often generate outward reaction forces and uneven pressures, whereas the proposed pre-shaping and finger sliding gripper leverages pre-shaping to equalize contact pressure and produce net inward forces that enhance pull-out resistance.

I. INTRODUCTION

Effective robotic harvesting of delicate fruits requires end-effectors capable of achieving grip stability while minimizing the risk of bruising and surface damage [1], [2]. However, conventional rigid grippers often generate localized stress on the fruit surface and require high positional accuracy, leading to frequent surface damage when operating in unstructured agricultural environments [3], [4]. To address these limitations, soft robotic grippers have gained increasing attention [5]. Their inherent passive compliance (PC), arising from the compliance of the soft materials, the geometric slenderness of the fingers, and the elastic properties of the underlying structures, enables improved surface conformity and more distributed contact forces, reducing localized stress peaks [6], [7]. However, passive compliance often limits the achievable gripping force and pull-out resistance required during harvesting.

Several soft gripper strategies have been proposed. Fin Ray effect fingers offer high compliance and adaptability[8], [9], but their structural softness can limit grasp stability when handling large or heavy products [10]. Underactuated tendon-driven fingers with PC similarly mitigate bruising [11], but the distributed force transmission across joints constrains the maximum controllable gripping force [12], [13]. Recent efforts also investigate reconfigurable multi-finger architecture to improve versatility in agri-food manipulation[14], including a reconfigurable four finger gripper, adaptable to different fruit shapes and task purposes [15]. Recent works have also explored pressure equalization and conformal grasping through structural compliance at the contact interface, for instance by employing metamaterial-inspired gripper designs or phalanges with adaptive or variable stiffness[16], [17]. These approaches primarily rely on passive deformation or local stiffness modulation to distribute contact loads and improve grasp robustness. In contrast to these representative approaches, handed-shearing auxetic (HSA) actuators provide a compact and electrically driven solution for compliant finger design [18]. In HSA structures, motor torque is converted from torsion to axial extension and, through geometric constraints, into controlled bending [19]. This enables active shape modulation while preserving intrinsic compliance [20], [21]. In the proposed design, a single HSA cylinder is adopted for each gripper finger.

Human grasping behavior provides an additional design

This work was supported by FISA-2023-00358, Horizon Europe Research and Innovation Programme INTELLIMAN (G.A. 101070136), AI-AGRI-HAND (BIITASRB24_00187) and euROBIN (G.A. 101070596).

X. Zhang is affiliated with both the Department of Mechanical Engineering, University of Genoa, 16145 Genoa, Italy, and the TUM School of Computation, Information and Technology and the Munich Institute of Robotics and Machine Intelligence (MIRMI), Technical University of Munich, 80333 Munich, Germany (e-mail: xiaoqian.zhang@edu.unige.it).

M. Baggetta and G. Berselli are with the Department of Mechanical Engineering, University of Genoa, 16145 Genoa, Italy.

C. Piazza is with the TUM School of Computation, Information and Technology and the Munich Institute of Robotics and Machine Intelligence (MIRMI), Technical University of Munich, 80333 Munich, Germany.

Corresponding author: Cristina Piazza (cristina.piazza@tum.de) and Giovanni Berselli (giovanni.berselli@unige.it).

principle. Neurophysiological studies show that during reach-to-grasp, the hand anticipatorily adjusts its configuration to match target geometry before contact - a phenomenon known as pre-shaping (PS) [22], [23], [24]. This anticipatory adaptation increases initial contact area and geometric alignment, improving grasp stability without requiring excessive force. Translating this concept to robotic manipulation suggests that combining active PS with PC can maintain higher gripping forces while still avoiding bruising [25].

Building on these principles, we propose a PS self-centering soft gripper that combines finger sliding (FS) with active curvature control through pre-shaping. As shown in Fig. 1, all fingers translate along linear guides in a parallel and self-centering configuration, adapting to object size while maintaining near-normal contact orientations relative to the fruit surface. This reduces outward reaction components that can destabilize the grasp. Simultaneously, the PS mechanism actively adjusts finger curvature prior to contact, improving geometric conformity and generating a more uniform pressure profile compared to relying on passive compliance alone. The inward curved preshaped configuration naturally encloses the object, increasing pull-out resistance during harvesting without increasing the clamp force compared to PC-only gripping. The PS function is realized through HSA-based fingers, which combine compliance with structural strength. In the proposed implementation, the load paths for sliding and bending are mechanically decoupled, avoiding the frictional coupling inherent to traditional rotational HSA actuation.

Finite element simulations demonstrate that PS produces a more uniform contact pressure distribution compared to PC alone. Experimental validation with the proposed gripper shows increased pull-out resistance while maintaining low levels of fruit damage. Together, these results indicate the potential to combine active PS with compliant structural motifs for robotic harvesting end effectors.

The rest of the paper is organized as follows: Sec. II describes the design methodology and operating principle. Sec. III presents the finite element simulation results. Sec. IV describes the experimental validation, while Sec. V presents the results. Finally, Sec. VI concludes with a discussion of the findings and potential future developments.

II. METHODS

The proposed gripper, shown in Fig. 2 consists of three parts: the control and drive module, the FS mechanism for linear feeding of the gripper, and the PS mechanism for controlling the finger bending. The chassis is 3D printed using PLA material, and the HSA-inspired fingers are made in FILOFlex TPU 90 A.

A. Principle of PS and FS Gripper Mechanisms

The FS and PS are independent of each other at the control level, but geometrically coupled at the mechanism level, so that the PS can be triggered from any FS clamping position, and the PS can be synchronized to drive all three fingers by a single servomotor. This architecture aims to:

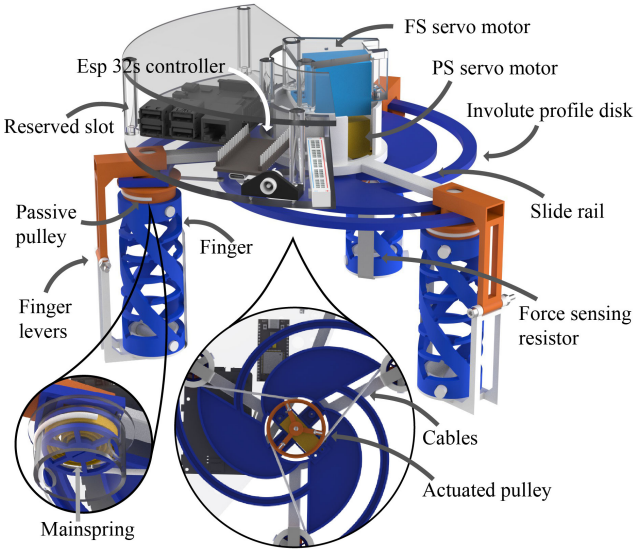

Fig. 2. CAD design of the proposed gripper, with actuation mechanisms and main components highlighted.

reduce the overall mass of the gripper (especially at the end), complete the PS before clamping, and maintain the formed PS attitude during the FS feed, in order to achieve the homogenization of the pressure distribution as desired in the previous simulation.

The upper part is the control and drive module, which adopts Node ESP32s as the master control, and is responsible for driving the FS servomotor, PS servomotor (Bluebird BLS-A930+), and the testing servomotor (not shown in the Figure). At the same time, it collects the return pressure of the FSR (force sensitive resistor) on the inner side of the three fingers, as well as the tension data from the load cell (not shown in the Figure). The FSR model is ZD10-100 with a range of 0-10 kg. The control area is reserved for interfaces and mounting of other controllers (e.g., Raspberry Pi systems) for subsequent iterations and upgrades.

The PS system is realized with three HSA fingers, where each finger integrates an HSA cylinder originally proposed as a compliant actuator (twist to extension, here constrained to bending) and is used directly as the grasping interface. This design enables active curvature pre-shaping with a controllable bending amplitude while preserving passive compliance at contact, and provides a lightweight, monolithic soft structure that promotes surface conformity and pressure homogenization compared with conventional rigid-link or purely passive soft fingers. Each finger consists of a finger lever that translates along the slide rail, a passive pulley that rotates the upper part of the finger tip, and the HSA-based finger that acts as a flexible actuator. The actuated pulley in the middle of the gripper is actuated by the cable: when the cable is actively tightened, the passive pulleys rotate passively clockwise under traction, resulting in an axial shortening of the finger. Since the finger lever is limited to a single degree of freedom of rotation at the central joint, this axial shortening is converted into finger bending, which

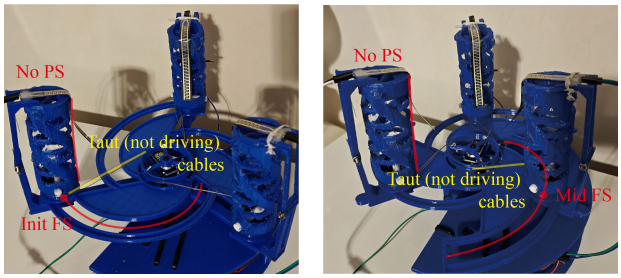

(a) FS at init-travel, PS inactive, cables taut no driving

(b) FS at mid-travel, PS inactive, cables taut no driving

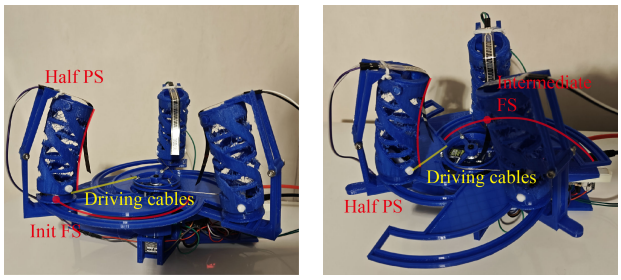

(c) FS at init-travel, PS at half-stroke, cables driving

(d) FS at near-end-travel, PS at half stroke, cables driving

Fig. 3. Prototype states illustrating the coupled finger sliding (FS) and pre-shaping (PS) operation across the involute-disk stroke.

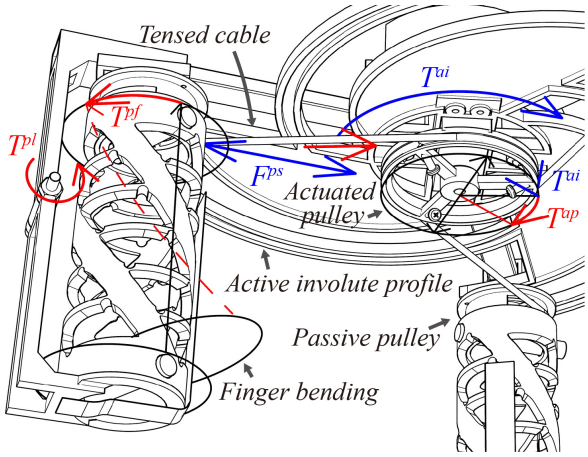

(a) Mechanics analysis of the PS-FS system

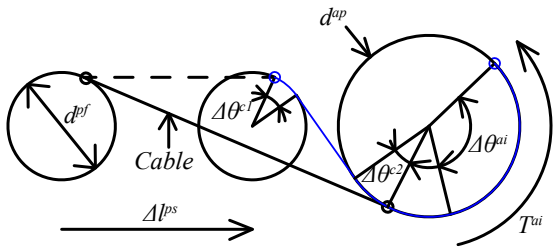

(b) FS coupling with taut but non-driving cable

Fig. 4. Mechanics and kinematics of the pre-shaping and finger sliding system.

realizes the PS. Therefore, the degree of finger bending is determined by the amount of cable retraction, and the PS amplitude can be set according to the curvature of the target surface (manually preset in this study). Since it is difficult for the finger flexible structure to return to the initial position by its own elasticity after the cable is untensioned, a mainspring is integrated into the passive pulley to provide the return torque to ensure that the finger is upright and repeatable in the initial state.

For the FS system, the PS servomotor is mounted on the involute profile disk, so when the FS servomotor drives the disk, the PS servomotor co-rotates with the disk; each finger lever slides linearly along the slide rail on one end, and engages/follows the involute slide rail on the other end via a roller/pin. The result:

On the one hand, according to the geometrical transmission characteristics of the involute groove, the three fingers are fed along the slide rail at approximately constant speed when the FS servomotor is rotating at constant speed;

On the other hand, by selecting the diameter of the actuated pulley, and when the PS servomotor maintains the initial angular position, the linear displacement of the slide rail and the angular displacement of the active pulley form a matching coupling, so that in the full stroke of the involute profile disk, the cable is always kept in tension and the constraints of “taut but non-driving”. Thus, the PS action can be triggered and maintained stably in any FS clamping position.

Figure 3 shows two typical states of the prototype based on the above principle: Fig. 3(a) and (b) show the FS moving to about the middle of the involute groove (or slide) with no PS activation, the cables remain taut but not driving. Since the cable remains taut throughout the entire stroke without driving the passive pulley, any PS setting of any amplitude can be achieved at any position of the FS stroke, thus realizing the gripping process of ”aligning, then wrapping, and maintaining preforms while advancing”; Fig. 3(c) and (d) show the FS moving near the end of the stroke with the finger about halfway PS, the cables continue driving the PS to the same degree throughout the FS move.

B. Force and kinematic analysis

This subsection analyzes the transmission of actuation torque to finger bending and the kinematic coupling between rotational actuation and linear finger sliding in the PS-FS mechanism. We denote quantities associated with the actuated pulley by the superscript *ap*, those associated with the passive finger by *pf*, and those associated with the passive linkage by *pl*. Fig. 4 further illustrates the force analysis of the PS-FS mechanism and the operating principle of the FS coupling. In the mechanics analysis diagram of Fig. 4(a), the mainspring is housed in the passive pulley as a preload torque acting on the passive side.

Under quasi-static, no slip assumptions (neglecting inertia and cable self weight), let the pulley radii be $r^{ap} = d^{ap}/2$ and $r^{pf} = d^{pf}/2$, and denote the cable transmission effi-

ciency by $\eta_c \in (0, 1]$. The torque T^{ap} on the actuated pulley produces a cable tension

$$F_c = \frac{\eta_c T^{ap}}{r^{ap}} = \frac{2\,\eta_c}{d^{ap}} T^{ap}. \tag{1}$$

The passive pulley experiences cable force, the mainspring preload, and bearing/axle friction. Let the mainspring preload torque be T_0^{ms} and the equivalent passive side friction torque be M_{fr}^{pf}. Then

$$T^{pf} = F_c\, r^{pf} - T_0^{ms} - M_{fr}^{pf} = \eta_c \frac{d^{pf}}{d^{ap}} T^{ap} - T_0^{ms} - M_{fr}^{pf}. \tag{2}$$

Through the linkage and proximal joint, T^{pf} is transformed into the finger-base bending torque T^{pl}. With an equivalent transmission ratio $\gamma(\theta)$ (input: passive pulley shaft; output: finger base joint), we have

$$T^{pl} = \gamma(\theta)\, T^{pf}. \tag{3}$$

Denote the total load on the finger side as

$$T^{ld}(\theta) = T^{HSA}(\theta) + T^{grip}(\theta) + M_{fr}^{pl}, \tag{4}$$

where the three terms correspond to HSA deformation, grip loading, and joint friction, respectively. The equilibrium $T^{pl} = T^{ld}$ yields a lower bound requirement for the actuated side torque:

$$T^{ap} \geq \frac{d^{ap}}{\eta_c\, d^{pf}} \left(\frac{T^{ld}(\theta)}{\gamma(\theta)} + T_0^{ms} + M_{fr}^{pf} \right). \tag{5}$$

For the FS chain, the involute disk maps the disk rotation ϕ to the rail displacement via the base radius R_b:

$$x(\phi) = R_b\, \phi \quad \text{(ideal geometry)}. \tag{6}$$

In our design, $\phi_{tot} = 120^\circ = 2\pi/3$ and $x_{tot} = 70\,\text{mm}$, which gives $R_b = 70/(2\pi/3) \approx 33.42$ mm. Let the constant sliding friction along the rail be F_{fr} and the disk shaft friction be M_{fr}^{ai}. The FS torque balance then gives the equivalent thrust along the rail

$$F^{fs} = \frac{T^{ai} - M_{fr}^{ai}}{R_b} - F_{fr}. \tag{7}$$

The coupled motion of Fig. 4(b) is analyzed with a "taut but non-driving cable" constraint. Let d^{ap} and d^{pf} be the diameters of the actuated and passive pulleys, respectively ($r^{ap} = d^{ap}/2$, $r^{pf} = d^{pf}/2$). When the actuated pulley rotates by $\Delta\theta^{ai}$, the rail undergoes a displacement Δl^{ps}. Define the additional wrap angle increments caused by the passive pulley approaching the actuated pulley and by tangency migration as $\Delta\theta^{c2}$ (on the actuated side) and $\Delta\theta^{c1}$ (on the passive side), taking positive values for increasing wrap. Cable length compatibility gives

$$\begin{aligned} \Delta l^{ps} &= r^{ap}\left(\Delta\theta^{ai} + \Delta\theta^{c2}\right) + r^{pf}\,\Delta\theta^{c1} \\ &= \tfrac{d^{ap}}{2}\left(\Delta\theta^{ai} + \Delta\theta^{c2}\right) + \tfrac{d^{pf}}{2}\,\Delta\theta^{c1}. \end{aligned} \tag{8}$$

On the other hand, the involute coupling imposes

$$\Delta l^{ps} = R_b\, \Delta\theta^{ai}. \tag{9}$$

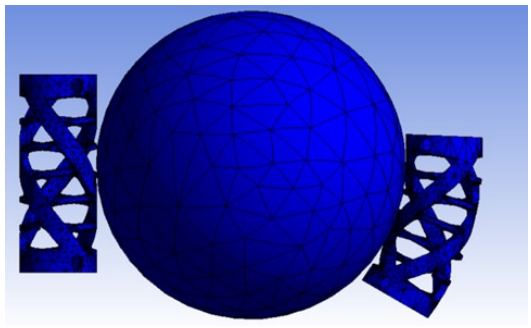

(a) Simulation setup

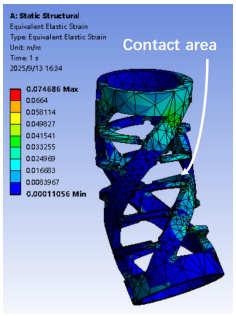

(b) Pre-shaping mode

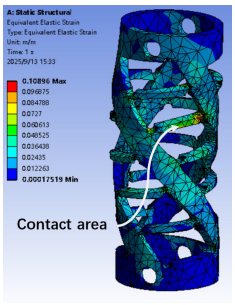

(c) Passive compliance mode

Fig. 5. FEM simulation in Ansys 2022 for pressure distribution acquisition when gripping, (a) initial setup of the simulation, and the results of gripping in (b) Pre-shaping mode, and (c) Passive compliance mode.

Combining (8) and (9) yields the total wrap-angle constraint

$$r^{ap}\,\Delta\theta^{c2} + r^{pf}\,\Delta\theta^{c1} = \left(R_b - r^{ap}\right)\Delta\theta^{ai}, \tag{10}$$

or, in diameter form,

$$\tfrac{d^{ap}}{2}\,\Delta\theta^{c2} + \tfrac{d^{pf}}{2}\,\Delta\theta^{c1} = \left(R_b - \tfrac{d^{ap}}{2}\right)\Delta\theta^{ai}. \tag{11}$$

These equations unify the drive rotation rail displacement relation ($\Delta\theta^{ai} \leftrightarrow \Delta l^{ps}$) with the wrap angle corrections ($\Delta\theta^{c1}, \Delta\theta^{c2}$) in a single loop constraint. Given d^{ap}, d^{pf}, R_b, specifying any one of the angle increments determines the others and closes the kinematic solution. For differential use in numerical integration or small motion linearization,

$$\mathrm{d}l^{ps} = r^{ap}\left(\mathrm{d}\theta^{ai} + \mathrm{d}\theta^{c2}\right) + r^{pf}\,\mathrm{d}\theta^{c1} = R_b\,\mathrm{d}\theta^{ai}. \tag{12}$$

III. Contact Pressure Simulation

A static structural simulation based on ANSYS was performed to simulate the contact pressure distribution of both PS and PC grippers when clamping a target; the same clamping force and boundary settings were maintained for both sets of conditions. The evaluation metrics focus on the uniformity of the pressure distribution, which is used to verify early in the design process the potential advantages of the PS gripper over the PC only gripper in terms of fruit loss reduction and the necessity of PS.

As in Fig. 5(a), the test target is a small ball of 80 mm diameter, set in PLA (this diameter refers to the common size of larger apples). The left side shows the clamping condition when the solution is not preformed (initial state, which can

be regarded as a PC gripper), and the right side shows the condition when the PS is actuated by the drive mechanism of the solution, whose curvature is adjusted to match the curvature of the surface of the ball within the reachable travel range of the prototype. In order to eliminate the interference of positioning factors, the positions of both grippers with respect to the ball were adjusted to be ideally aligned (with the total force direction pointing approximately to the center of the ball). Both grippers were made of TPU-90 A and modeled as a near-incompressible isotropic elastic material ($E = 3.37\times10^7$ Pa, $\nu = 0.487$) , with fixed constraints at the upper and lower ends (consistent with the prototype design). The loading method was to apply an equivalent reverse force of 20 N in the horizontal direction on the left and right sides of the ball to simulate the clamping action equivalently. The contact between the ball and the fingers was modeled as frictionless, as the analysis focuses on the normal contact pressure distribution and relative sliding is limited under the applied loading, while avoiding additional uncertainty from friction coefficients.

As can be seen in Fig. 5(b) and Fig. 5(c), the PS case has a significantly more uniform contact pressure distribution with a lower peak pressure, while the PC case has a slightly larger contact area, but the pressure is more concentrated in the middle of the contact area (i.e., the starting area of the passive press in). This suggests that the curvature based pre-fitting of the PS helps to achieve a more even pressure at the contact moment, thus reducing the risk of fruit damage due to localized high pressure.

Despite the excellent PC properties of the HSA structure, it is difficult to achieve "high clamping force + pressure homogenization" at the same time by relying on the PC alone: increasing the structural stiffness increases the clamping force, but it also raises the local pressure and increases the risk of fruit damage. In contrast, combining PS with PC alters the contact boundary conditions at the moment of touch by pre-matching curvature, enabling pressure homogenization and higher pull-out resistance under the same clamping load. This underscores the fundamental design advantage of incorporating active PS in conjunction with passive compliance mechanisms.

IV. Experiments

Guided by the hypothesis that, relative to PC grippers, a PS gripper can leverage curvature pre-alignment to equalize contact pressures while increasing pull-out resistance, a dedicated pull-out test rig was developed (Fig. 6). On the upper stage, a fishing line is wound around the motor output shaft, and its free end is centrally tied to one measurement side of a load cell (XJC-S09-B-5 kg). On the lower stage, a second fishing line connects the opposite side of the load cell to the gripped target. The testing motor is positioned such that the fishing line passes vertically through the geometric center of the gripper's top cover, while the gripper faces upwards. The bottom cover is fastened at the geometric center of the test platform. This coaxial configuration ensures that the center of mass of the target is nominally

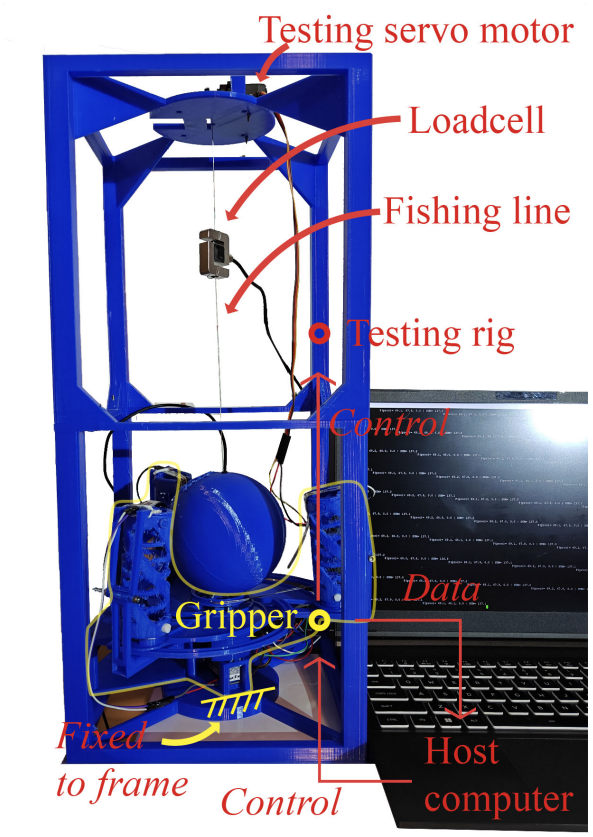

Fig. 6. Pull-out test rig: MG996R (360°) testing servo, centrally routed fishing line, in-line load cell (XJC-S09-B-5 kg), and upward-facing gripper.

aligned with the gripper's central axis, minimizing off-axis moments. During trials, the testing servo motor rotates at constant speed to lift the sphere vertically. Both motor actuation and load cell data acquisition are managed by the gripper side ESP32 controller.

As shown in Fig. 7, two operating modes are evaluated: PC and PS, both following a grip-pull-out protocol. First, the drop height of the target is adjusted so that the object enters the gripping envelope without contacting the fingers (Fig. 7a,b). Before each trial, the gripper and sensors are initialized, and all servos are returned to their home position. The FSR signals from the inner surfaces of the three fingers are multi-sample averaged, then log transformed and normalized to reduce noise and improve resolution at low pressure. This also helps maintain consistent clamp force across modes. The load cell signal (acquired via an HX711 amplifier) is calibrated and recorded as raw data for subsequent analysis. Since prior characterization showed that HSA elements exhibit a higher peak output during initial cycles before stabilizing to a practical operating level after approximately 20 full-stroke cycles, a pre-conditioning phase in each mode is introduced. Before recording experimental data, the gripper performs 30 maximum force grips to stabilize the mechanical behaviour. This is followed by 10 recorded trials under identical conditions. In PC mode, the gripper performs FS clamping without activating

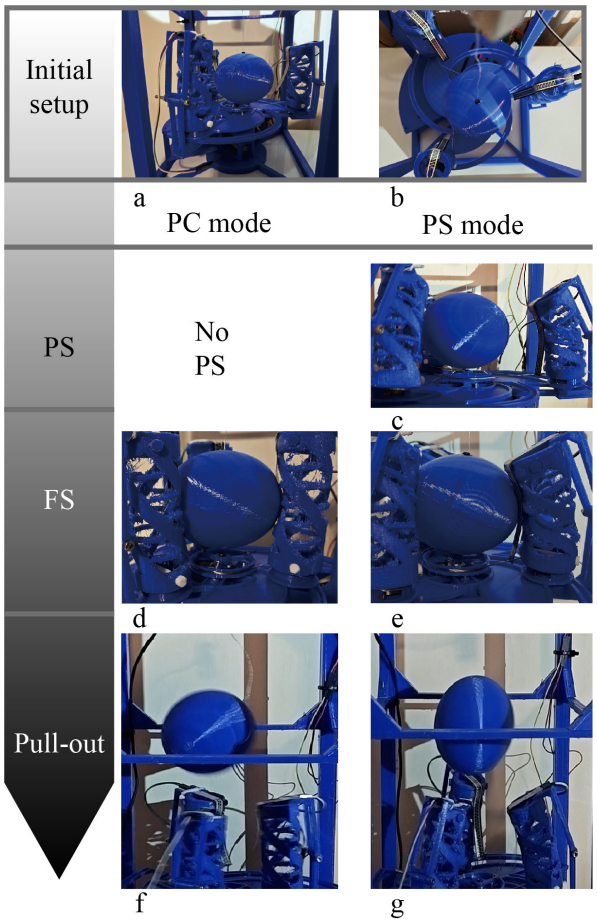

Fig. 7. Passive compliance vs. pre-shaping grip–pull-out protocol and typical sequences. Panels (a)–(g) are embedded in the figure.

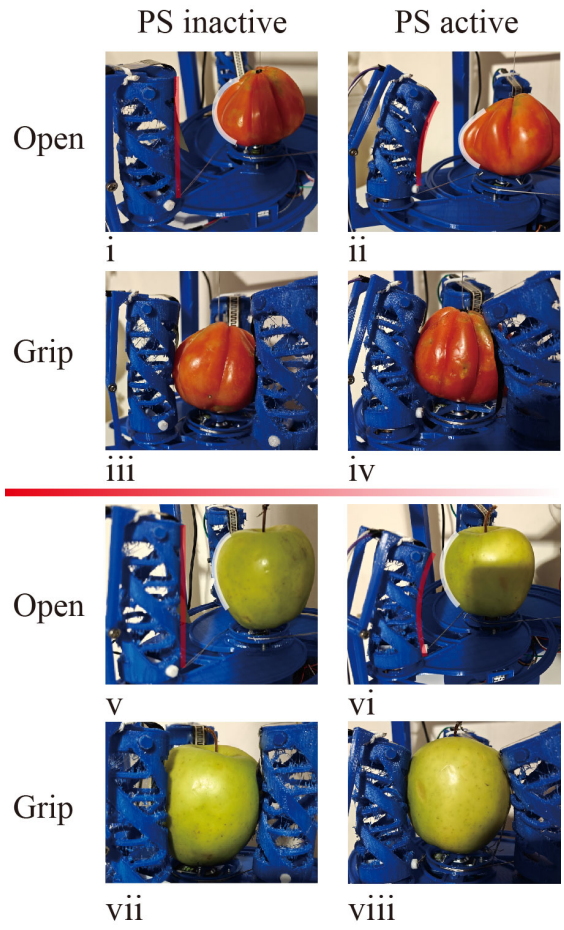

Fig. 8. The comparison of the grip in pre-shaping and pre-shaping inactive modes of tomato and apple.

the PS mechanism. Clamping stops when the sum of the three processed FSR readings (post processing) reaches a set point of 15 N (Fig. 7d). Then pull-out motor is activated at constant speed, and the pull-out force is recorded from the instant the 15 N clamping threshold is reached until complete detachment of the sphere (bounce out, Fig. 7f). In PS mode, the gripper first executes a manually preset PS command (servo position for cable driven) according to the estimated surface curvature of the target (Fig. 7c). After PS, then the mechanism clamps the target to the same 15 N summed FSR set point (Fig. 7e). The pull-out is then performed identically to the PC condition, and force data are recorded until complete detachment (bounce out illustrated in Fig. 7g).

V. Results

To qualitatively illustrate the effect of PS on objects of different geometries, grasping trials were conducted on an irregular tomato and a more regular apple (Fig. 8). The first grasping stage demonstrates the geometric function of PS. As shown in Fig. 8(ii,vi), when PS is enabled, the fingers actively bend prior to contact to match the surface curvature of the fruit. In contrast, in Fig. 8(i,v), without PS, conformity only arises passively during gripping. Thus, during the grip phase, Fig. 8(iv,viii) show a closer geometric fit and increased contact area compared to Fig. 8(iii,vii). These qualitative observations are consistent with the finite element simulations and suggest that PS should lead to increased pull-out resistance in subsequent quantitative tests.

Quantitative results from the pull-out experiments are presented in Fig. 9. For each mode (PC and PS), 10 trials were processed and analyzed. The full time histories of the summed finger pressures and the pull-out force are plotted. The stage labels d/f/e/g correspond to the phases illustrated in Fig. 7. Since the load cell provides raw tension reading, the signal was sign-corrected (a convention for tension to be negative) and scaled according to calibration factors to obtain the final pull-out force values. Gripping and pulling were executed continuously within the control program. Immediately after clamping, the target's pose undergoes minimal change; therefore, the initial tension state of the fishing line at the onset of pulling cannot be precisely determined. Moreover, the exact onset of the pull-out motion cannot be precisely defined in the force trace due to the flexibility of the TPU. Based on real time observations, a steady sliding window (approximately 6.8 s) was selected and set as the comparison

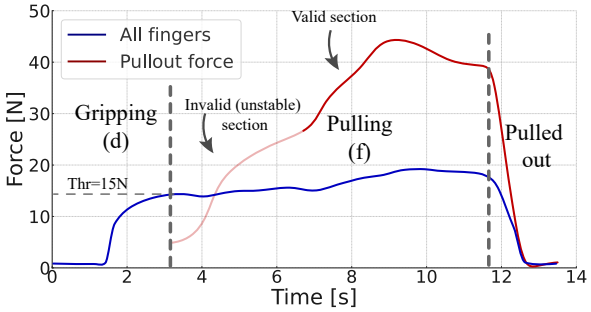

(a) Passive compliance mode

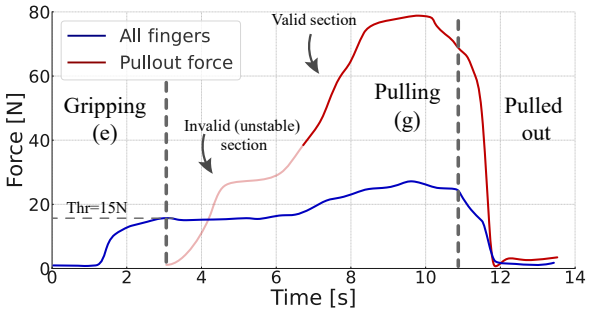

(b) Pre-shaping mode

Fig. 9. Sum of three finger pressures and pull-out force vs. time for passive compliance and pre-shaping modes. Stage tags d/f/e/g correspond to the phases illustrated in Fig. 7.

interval for force analysis.

In Fig. 9(a) (corresponding to PC mode), once the summed finger pressure reaches 15 N set point, the FS mechanism maintains a fixed position. As the target is pulled upward, the contact region transitions toward the stiffer distal portion of the fingers. The maximum pull-out force reaches approximately 44 N. At this stage, the total measured finger pressure increases by about 5 N relative to the initial 15 N clamp force, reflecting the higher structural stiffness near the distal finger region. Overall, the force evolution during pull-out is relatively smooth.

In contrast, Fig. 9(b) shows the PS mode under the same initial pressure setting. The pull-out begins after establishing the same pressure setting. Due to curvature pre-alignment, once the target fully mates with the pre-bent finger segments, the effective contact area increases substantially. This results in a significantly larger rise in total contact pressure during pulling and a maximum pull-out force approaching 80 N. Moreover, the enveloping geometry produced by PS leads to a shorter pull-out stroke, with detachment occurring earlier than in PC mode. These results indicate that active pre-shaping substantially enhances pull-out resistance compared to passive compliance alone, while maintaining the same nominal clamping force.

VI. Discussion and Future Work

This work is situated in the domain of pre-contact curvature alignment. The FS mechanism provides controlled, parallel linear feeding so that pre-contact loading remains approximately normal to the fruit surface, while the PS mechanism establishes finger curvature before contact, creating an inherent geometric pre-alignment with the object. Both experimental and computational results support the effects observed under the same initial clamping force setting used in PC mode. In particular, PS systematically produced lower and more uniform pressure peaks, while during pull-out the enveloping contact geometry increased resistance to pull-out forces. Essentially, PS does more than simply introduce additional bending. It alters the boundary conditions of contact at the point of interaction through an ”align-contact-lock” process. This mechanism allows gentle initial contact while simultaneously ensuring stable contact retention.

The PS mechanism can be interpreted relative to designs that rely on only PC from two complementary perspectives, involving both surface kinematics and the mechanics of form closure. First, the PS distributes the contact line over a curved surface, increasing the overall contact area. For a given total clamping force, this reduces the pressure per unit area and therefore decreases the risk of surface damage. Second, PS decouples the function of FS (parallel sliding) and PS (control on curvature), allowing the gripper to preserve normal load components and suppress unfavorable tangential/outward components. This improves pull-out resistance without requiring an increase in peak contact pressure. These mechanisms explain the observed combination of smoother pressure traces and significantly higher pull-out forces in PS mode.

In this work, all quantitative results are obtained primarily from a spherical object tested under a coaxial pull-out scheme. This setup was selected to clearly separate and quantify the mechanical effect of PS while keeping the clamping force level consistent across tests. Future work will expand this evaluation to cover more comprehensive robustness experiments, e.g., tests on highly irregular, non-spherical or elongated fruits and vegetables, as well as off-center grasping conditions. These extensions will likely require a perception-guided PS adjustment and further underactuated design improvements.

The prototype also introduces practical engineering challenges. The 3D-printed chassis introduces assembly tolerances and limited global stiffness, which can lead to backlash and elastic deformation at several joints. The finger lever shown in Fig. 2 exhibits torsional deformation along the HSA axis, which partially reduces transmission efficiency and limits the achievable force peaks. Furthermore, some rotational interfaces currently operate without bearings, introducing unnecessary friction and additional elastic losses. The cable-driven PS mechanism may also alter the effective timing of contact during certain portions of the stroke or increase apparent structural stiffness. These factors likely contribute to the trials in which the measured clamping and pull-out forces did not reach their theoretical maxima.

In light of these observations, future work will focus on a co-design of mechanism geometry and control strategies. From the mechanical perspective, improvements will target increased structural stiffness, tighter manufacturing tolerances, optimized cable routing, and improved pulley sizing in

order to enhance transmission efficiency and reduce friction losses. From the geometry side, the design will incorporate parameterized models of PS kinematics and mechanics, including bending stroke range, virtual rotation center placement, torque transmission capacity, and the efficiency with which actuator torque is converted into gripping and pull-out forces. These models will enable systematic comparisons between different HSA actuation topologies, such as single-cable, multi-cable, differential cable arrangements, and parallel actuation strategies. On the control side, we will investigate higher-bandwidth force-position hybrid control with online curvature estimation and adaptive PS; in the present study, PS is manually preset to isolate the mechanical effect of pre-shaping. Furthermore, we plan to carry out systematic real-life grasping and damage evaluation experiments on fruits to fully verify the gripper's performance in practical harvesting scenarios. Future trials will assess robustness across broader fruit size, shape distributions, and compare with other similar soft gripper solutions.

REFERENCES

[1] Q. Wang, Y. Tu, W. Xu, J. Zhang, A. Knoll, M. Zhou, and Y. Ying, "Towards Damage-Less Robotic Fragile Fruit Grasping: A Systematic Review on System Design, End Effector, and Visual and Tactile Feedback," *Journal of Field Robotics*, p. rob.70021, Jul. 2025. [Online]. Available: https://onlinelibrary.wiley.com/doi/10.1002/rob.70021

[2] X. Wang, H. Kang, H. Zhou, W. Au, M. Y. Wang, and C. Chen, "Development and evaluation of a robust soft robotic gripper for apple harvesting," *Computers and Electronics in Agriculture*, vol. 204, p. 107552, Jan. 2023. [Online]. Available: https://linkinghub.elsevier.com/retrieve/pii/S0168169922008602

[3] K. Chen, T. Li, T. Yan, F. Xie, Q. Feng, Q. Zhu, and C. Zhao, "A Soft Gripper Design for Apple Harvesting with Force Feedback and Fruit Slip Detection," *Agriculture*, vol. 12, no. 11, p. 1802, Oct. 2022. [Online]. Available: https://www.mdpi.com/2077-0472/12/11/1802

[4] J. Shintake, V. Cacucciolo, D. Floreano, and H. Shea, "Soft Robotic Grippers," *Advanced Materials*, vol. 30, no. 29, p. 1707035, Jul. 2018. [Online]. Available: https://onlinelibrary.wiley.com/doi/10.1002/adma.201707035

[5] C. Piazza, G. Grioli, M. G. Catalano, and A. Bicchi, "A century of robotic hands," *Annual Review of Control, Robotics, and Autonomous Systems*, vol. 2, no. 1, pp. 1–32, 2019.

[6] M. Manti, T. Hassan, G. Passetti, N. d'Elia, M. Cianchetti, and C. Laschi, "An Under-Actuated and Adaptable Soft Robotic Gripper," in *Lecture Notes in Computer Science*. Cham: Springer International Publishing, 2015, pp. 64–74, iSSN: 0302-9743, 1611-3349. [Online]. Available: https://link.springer.com/10.1007/978-3-319-22979-9_6

[7] D. Zhang, W. Zhang, H. Yang, and H. Yang, "Application of Soft Grippers in the Field of Agricultural Harvesting: A Review," *Machines*, vol. 13, no. 1, p. 55, Jan. 2025, publisher: MDPI AG. [Online]. Available: https://www.mdpi.com/2075-1702/13/1/55

[8] S. Terrile, L. Y. Lee, and J. Rossiter, "Multigraingripper: Enhancing finray soft grippers to grasp granular material," in *2025 IEEE 8th International Conference on Soft Robotics (RoboSoft)*, 2025, pp. 1–6.

[9] R. M. Hartisch and K. Haninger, "High-speed electrical connector assembly by structured compliance in a finray-effect gripper," *IEEE/ASME Transactions on Mechatronics*, vol. 29, no. 2, pp. 810–819, 2024.

[10] A. Carloni, M. Valori, F. Bertolucci, L. Agostini, G. Berselli, I. Fassi, L. M. Tosatti, and R. Vertechy, "Enhancing compliant gripper performance: Exploiting electro-adhesion to increase lifting force over grasping force," *Robotics and Computer-Integrated Manufacturing*, vol. 91, p. 102843, 2025. [Online]. Available: https://www.sciencedirect.com/science/article/pii/S0736584524001303

[11] S. M. Kargar and G. Berselli, "TriCoM Gripper–Part II: Soft Pad Integration and Virtual Prototyping for Delicate Object Handling," in *2024 20th IEEE/ASME International Conference on Mechatronic and Embedded Systems and Applications (MESA)*. Genova, Italy: IEEE, Sep. 2024, pp. 1–6. [Online]. Available: https://ieeexplore.ieee.org/document/10704833/

[12] M. Bluiminck and W. Roozing, "An Underactuated Tendon-Driven Gripper with Variable Stiffness for Deformable Agri-Food Objects," in *2023 IEEE 19th International Conference on Automation Science and Engineering (CASE)*. Auckland, New Zealand: IEEE, Aug. 2023, pp. 1–8. [Online]. Available: https://ieeexplore.ieee.org/document/10260297/

[13] J. F. Elfferich, D. Dodou, and C. D. Santina, "Soft Robotic Grippers for Crop Handling or Harvesting: A Review," *IEEE Access*, vol. 10, pp. 75 428–75 443, 2022, publisher: Institute of Electrical and Electronics Engineers (IEEE). [Online]. Available: https://ieeexplore.ieee.org/document/9829727/

[14] J. H. Low, P. M. Khin, Q. Q. Han, H. Yao, Y. S. Teoh, Y. Zeng, S. Li, J. Liu, Z. Liu, P. Valdivia Y Alvarado, I.-M. Chen, B. C. K. Tee, and C. H. Yeow, "Sensorized Reconfigurable Soft Robotic Gripper System for Automated Food Handling," *IEEE/ASME Transactions on Mechatronics*, vol. 27, no. 5, pp. 3232–3243, Oct. 2022. [Online]. Available: https://ieeexplore.ieee.org/document/9550783/

[15] M. Baggetta, O. Pennacchio, S. Pirozzi, and G. Berselli, "A reconfigurable four-finger gripper for versatile application in the agri-food industry," *IEEE/ASME Transactions on Mechatronics*, vol. 30, no. 4, pp. 2999–3007, 2025.

[16] C. Tawk, R. Mutlu, and G. Alici, "A 3d printed modular soft gripper integrated with metamaterials for conformal grasping," *Frontiers in Robotics and AI*, vol. Volume 8 - 2021, 2022. [Online]. Available: https://www.frontiersin.org/journals/robotics-and-ai/articles/10.3389/frobt.2021.799230

[17] J. Zhou, Y. Chen, Y. Hu, Z. Wang, Y. Li, G. Gu, and Y. Liu, "Adaptive variable stiffness particle phalange for robust and durable robotic grasping," *Soft Robotics*, vol. 7, no. 6, pp. 743–757, 2020, pMID: 32319857. [Online]. Available: https://doi.org/10.1089/soro.2019.0089

[18] L. Chin, M. C. Yuen, J. Lipton, L. H. Trueba, R. Kramer-Bottiglio, and D. Rus, "A simple electric soft robotic gripper with high-deformation haptic feedback," in *2019 International Conference on Robotics and Automation (ICRA)*, 2019, pp. 2765–2771.

[19] I. Good, S. Balaji, and J. I. Lipton, "Torsion Resistant Strain Limiting Layers Enable High Grip Strength of Electrically-Driven Handed Shearing Auxetic Grippers," 2024, version Number: 1. [Online]. Available: https://arxiv.org/abs/2412.07976

[20] L. Chin, J. Lipton, R. MacCurdy, J. Romanishin, C. Sharma, and D. Rus, "Compliant electric actuators based on handed shearing auxetics," in *2018 IEEE International Conference on Soft Robotics (RoboSoft)*, 2018, pp. 100–107.

[21] R. L. Truby, L. Chin, and D. Rus, "A recipe for electrically-driven soft robots via 3d printed handed shearing auxetics," *IEEE Robotics and Automation Letters*, vol. 6, no. 2, pp. 795–802, 2021.

[22] C. R. Mason, J. E. Gomez, and T. J. Ebner, "Hand Synergies During Reach-to-Grasp," *Journal of Neurophysiology*, vol. 86, no. 6, pp. 2896–2910, Dec. 2001. [Online]. Available: https://www.physiology.org/doi/10.1152/jn.2001.86.6.2896

[23] C. Bard and J. Troccaz, "Automatic preshaping for a dextrous hand from a simple description of objects," in *EEE International Workshop on Intelligent Robots and Systems, Towards a New Frontier of Applications*, 1990, pp. 865–872 vol.2.

[24] M. Higashimori and M. Kaneko, "Design of joint spring for dynamic preshaping," in *Proceedings 2003 IEEE/RSJ International Conference on Intelligent Robots and Systems (IROS 2003) (Cat. No.03CH37453)*, vol. 3. Las Vegas, Nevada, USA: IEEE, 2003, pp. 2101–2106. [Online]. Available: http://ieeexplore.ieee.org/document/1249181/

[25] S. Hara, O. Fukuda, and M. Higashimori, "Juzu Type Gripper That Can Change Both Shape and Firmness," in *2025 IEEE International Conference on Robotics and Automation (ICRA)*. Atlanta, GA, USA: IEEE, May 2025, pp. 16 471–16 477. [Online]. Available: https://ieeexplore.ieee.org/document/11127377/